AGU PUBLICATIONS

Water Resources Research

RESEARCH ARTICLE
10.1002/2016WR019393

Tracer-based characterization of hyporheic exchange and benthic biolayers in streams

Julia L. A. Knapp[1,2], Ricardo González-Pinzón[3], Jennifer D. Drummond[4], Laurel G. Larsen[2,5], Olaf A. Cirpka[1], and Judson W. Harvey[2]

[1]Center for Applied Geoscience, University of Tübingen, Tübingen, Germany, [2]National Research Program, U.S. Geological Survey, Reston, Virginia, USA, [3]Department of Civil Engineering, University of New Mexico, Albuquerque, New Mexico, USA, [4]Integrative Freshwater Ecology Group, Center for Advanced Studies of Blanes (CEAB-CSIC), Blanes, Girona, Spain, [5]Department of Geography, University of California, Berkeley, California, USA

Key Points:
- In-stream tracer measurements specify bulk stream reactivity but not biolayer depth
- Streambed profiles identify reactive zones, but not contributions to whole-stream reactivity
- Coupled in-stream and multidepth measurements contextualize hyporheic and reach-scale processing

Supporting Information:
- Supporting Information S1

Correspondence to:
J. L. A. Knapp,
julia.knapp@uni-tuebingen.de

Citation:
Knapp, J. L. A., R. González-Pinzón, J. D. Drummond, L. G. Larsen, O. A. Cirpka, and J. W. Harvey (2017), Tracer-based characterization of hyporheic exchange and benthic biolayers in streams, *Water Resour. Res.*, *53*, doi:10.1002/2016WR019393.

Received 22 JUN 2016
Accepted 21 JAN 2017
Accepted article online 28 JAN 2017

Abstract Shallow benthic biolayers at the top of the streambed are believed to be places of enhanced biogeochemical turnover within the hyporheic zone. They can be investigated by reactive stream tracer tests with tracer recordings in the streambed and in the stream channel. Common in-stream measurements of such reactive tracers cannot localize where the processing primarily takes place, whereas isolated vertical depth profiles of solutes within the hyporheic zone are usually not representative of the entire stream. We present results of a tracer test where we injected the conservative tracer bromide together with the reactive tracer resazurin into a third-order stream and combined the recording of in-stream breakthrough curves with multidepth sampling of the hyporheic zone at several locations. The transformation of resazurin was used as an indicator of metabolism, and high-reactivity zones were identified from depth profiles. The results from our subsurface analysis indicate that the potential for tracer transformation (i.e., the reaction rate constant) varied with depth in the hyporheic zone. This highlights the importance of the benthic biolayer, which we found to be on average 2 cm thick in this study, ranging from one third to one half of the full depth of the hyporheic zone. The reach-scale approach integrated the effects of processes along the reach length, isolating hyporheic processes relevant for whole-stream chemistry and estimating effective reaction rates.

1. Introduction

River corridors convey water over and around fluvial features and exchange water across sediment interfaces, causing mixing between river water and groundwater that creates steep gradients in temperature, pH, redox conditions, and nutrient availability and thereby enhance chemical reactions [*Boulton et al.*, 1998; *Boano et al.*, 2014; *Harvey and Gooseff*, 2015]. River interactions with hyporheic zones are widely important for water quality and for creating unique habitats for aquatic organisms [*Stanford and Ward*, 1988; *Boulton et al.*, 1998; *Boano et al.*, 2014]. Chemical reactions in the hyporheic zone also contribute to the overall health and functions of the stream network, notably influencing nutrient cycling [*Grimm and Fisher*, 1984; *Bardini et al.*, 2012] and metabolic activity [*Brunke and Gonser*, 1997; *Krause et al.*, 2011]. However, not all parts of the hyporheic zone interact equally with the stream. Recently, it has been proposed that the shallow layer at the top of the streambed, or slightly beneath it, is an active area for biotic and abiotic chemical transformations [*Battin et al.*, 2003; *O'Connor and Harvey*, 2008]. This "shallow benthic biolayer" at the uppermost sediments accumulates organics (i.e., organic carbon and other fine particles), algae, periphyton, and microbes and thus influences redox zonation and hyporheic processes [*Boano et al.*, 2014; *Battin et al.*, 2016]. In this biolayer, microorganism abundances are often highest [e.g., *Navel et al.*, 2011; *Harvey et al.*, 2013] and mediate key biochemical reactions across the stream network [*Briggs et al.*, 2015], including aerobic respiration [*González-Pinzón et al.*, 2012, 2014], denitrification [*O'Connor and Hondzo*, 2008; *Harvey et al.*, 2013], and degradation of organic contaminants [e.g., *Conant et al.*, 2004]. Furthermore, environmentally relevant sorption and precipitation reactions take place in this layer [*Fuller and Harvey*, 2000], affecting the transport and reactivity of trace metals and nutrients [*Rodriguez-Freire et al.*, 2016]. The benthic biolayer is described as an extension of the surficial benthic biofilm deeper into the hyporheic zone (Figure 1a) and its

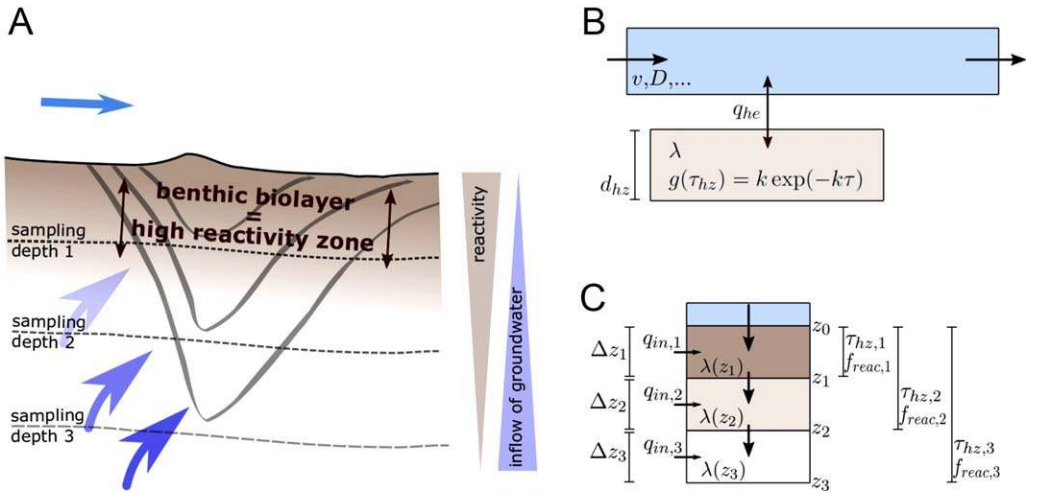

Figure 1. (a) Illustration of hyporheic exchange and reactivity: hypothetical hyporheic flow paths and the gradient of reactivity in the subsurface indicating the extent of the benthic biolayer; (b) conceptual representation of hyporheic processes by the transient storage model (Model I), which captures in-stream processes (advective velocity v, dispersion D, etc.) and assumes one single hyporheic storage zone with an exponential distribution of hyporheic residence times τ and linear reactivity in the hyporheic zone (transformation constant λ), but does not capture individual flow paths into and out of the hyporheic zone; (c) conceptual representation of processes captured by the subsurface model (Model II), which compartmentalizes the hyporheic zone into individual layers with distinct reactivity (transformation constants λ) and different contributions of groundwater (fluxes q_{in}), but only represents the vertical component of the downwelling flow paths, thus quantifying water ages at the different depths (i.e., τ_{hz}) and reaction ratios (f_{reac}), but making no assumptions about how, when and where the water returns to the stream. All parameters are explained in detail in section 2.

depth varies depending on flow and transport, grain-size, redox chemistry, carbon and nutrient sources, and biogeochemical reactions. Little is known about the vertical extent of biolayers, although several field studies identified a layer of some centimeters within a granular and permeable sediment matrix where hyporheic exchange occurred to a depth of tens of centimeters (see discussions in *Arnon et al.* [2013] and *Harvey et al.* [2013]). The potential importance of the benthic biolayer to reactive processing in river networks was highlighted in the recent modeling work by *Gomez-Velez et al.* [2015], who estimated that denitrification occurring beneath small-stream bedforms was of far greater importance to processing of nitrate in the upper Mississippi river than denitrification occurring in longer and deeper hyporheic flow paths through bars and meanders.

Hyporheic processes can be assessed on multiple spatiotemporal scales, from measurements and modeling approaches on the pore-scale (i.e., with microelectrodes) [*O'Connor et al.*, 2012] via studies on the centimeter-scale (e.g., with mini-piezometers) [*Harvey and Fuller*, 1998; *Briggs et al.*, 2013], to tracer-based investigations integrating the effects of hyporheic processes over longer stream reaches [*González-Pinzón et al.*, 2015], or even whole catchments [*Böhlke et al.*, 2009]. While in-stream tracer tests are a well-established tool for characterizing processes on the reach scale, there are fewer examples of measuring small-scale chemical gradients and reaction rates within the benthic biolayer [e.g., *O'Connor and Harvey*, 2008].

In recent years, coinjecting the reactive tracer resazurin into streams along with a conservative solute has become an established method to better understand the interactions between water and sediments [e.g., *Haggerty et al.*, 2008, 2009; *Argerich et al.*, 2011; *González-Pinzón et al.*, 2012; *Lemke et al.*, 2013a]. Resazurin is a fluorescent phenoxazine dye, which is reduced to fluorescent resorufin through reactions within living cells, among others, by aerobic microorganisms [*O'Brien et al.*, 2000; *González-Pinzón et al.*, 2012]. As the abundance of microorganisms in streams is the highest within the hyporheic zone [e.g., *Hendricks*, 1993; *Fischer et al.*, 1996], the transformation of resazurin can be utilized as an indicator of exchange processes with metabolically active transient storage zones [*Haggerty et al.*, 2008, 2009]. Resazurin could therefore potentially serve as a tracer of exchange and reaction within the benthic biolayer.

While results from localized sampling of the hyporheic zone are rarely representative of the general conditions of a greater stream section, reach-scale tracer investigations mainly provide information on bulk

reactivity without localizing where within the streambed the reaction is the greatest [*Harvey et al*., 2013]. Therefore, combining in-stream reactive tracer tests with sampling performed simultaneously in the hyporheic zone potentially improves the interpretation of the data, but there are only few studies in which reach-scale investigations of reactive transport in streams are coupled to detailed investigations within the hyporheic zone [e.g., *Harvey and Fuller*, 1998; *Böhlke et al*., 2009; *Harvey et al*., 2012, 2013]. This holds especially for the resazurin-resorufin tracer [*González-Pinzón et al*., 2015].

Figures 1b and 1c illustrate those aspects of hyporheic exchange and reactivity captured by in-stream and detailed subsurface sampling according to the modeling approaches used here. The measured in-stream concentrations reflect the part of the hyporheic processes that affect the stream itself, but from these data it is impossible to derive the spatial distribution of reactivity within the hyporheic zone. Hence, the transient storage model used to interpret these data (Figure 1b) yields effective bulk estimates of reactivity of an assumed single, fully mixed storage zone. While models with multiple storage zones exist [e.g., *Marion et al*., 2008; *Kerr et al*., 2013], localization of these zones is impossible from in-stream data only. The concentrations measured within depth profiles of the streambed, in contrast to in-stream data, reflect the internal structure of the hyporheic zone. The proposed subsurface model (Figure 1c) considers vertical advective-dispersive-reactive transport and compartmentalizes the hyporheic zone into individual layers, thereby identifying layers of higher and lower reactivity in the subsurface. These layers differ conceptually from the multiple storage zones mentioned above, as we incorporate transport from one layer to the next, whereas the multiple storage zones only interact with the stream. Conversely, the vertical profiles do not provide information on hyporheic water returning to the stream, and thus it is difficult to deduce the large-scale influence of the internal organization of the hyporheic zone on the stream water. These two pieces of information are complementary and cannot be interchanged.

The aim of the present study was to quantify the contribution of the shallow subsurface to reactive turnover within the hyporheic zone and thus quantify the extent of the benthic biolayer. For this, we injected resazurin into a third-order stream (Difficult Run, Virginia, USA) and simultaneously measured the concentrations of resazurin and resorufin in the surface water at several distances from the injection point and in vertical profiles at shallow depths in the streambed, thereby identifying layers of higher and lower reactivity by comparing the full depth of hyporheic exchange with the depth over which reactive turnover effectively takes place. We analyzed in-stream results with the traditional transient-storage model based on the advection-dispersion equation (similar to *Bencala and Walters* [1983]; *Runkel* [1998], but including turnover of the reactive tracer; cf. *Lemke et al*. [2013a]) and the vertical depth profiles with an advection-dispersion-reaction type of model. We show that the two observation methods and models provide information about different aspects of the same system and illustrate how this leads to very different predictions of hyporheic depth and time scales of hyporheic exchange.

2. Methods

2.1. Site Description

Our tracer experiment was conducted within the headwaters of Difficult Run (catchment area of 14 km^2) in Virginia, USA, in a 150 m long study reach with variable topography including riffles, runs, and pools. The geology in the region is dominated by gneiss and schist bedrock. The streambed sediments are mainly composed of coarse sand, gravel, and pebbles interspersed with a relatively fine silty matrix with a porosity of 0.39 (estimated based on 31 shallow core samples taken along the reach). The study reach has an average bed slope of 6‰ and an average channel width and water depth equal to 5.57 and 0.2 m, respectively. On the morning of the injection (13 July 2011), the discharge was 0.027 m^3/s (USGS stream gage 01645704). The conservative tracer bromide and reactive tracer resazurin were coinjected with a constant rate over a period of 5 h. A total of 7850 g of bromide and 187 g of resazurin (codissolved in 175 L of stream water) were injected during the experiment. The in-stream plateau concentrations of the conservative tracer reached 16.5 mg/L.

About 1 h after the injection ended, a thunderstorm caused a spate (peak $Q \cong 0.88$ m^3/s) and raised the stream water level by 26 cm. All tracer measurements were terminated 1 h 45 min after the injection stopped because sampling equipment could not withstand the spate and had to be removed.

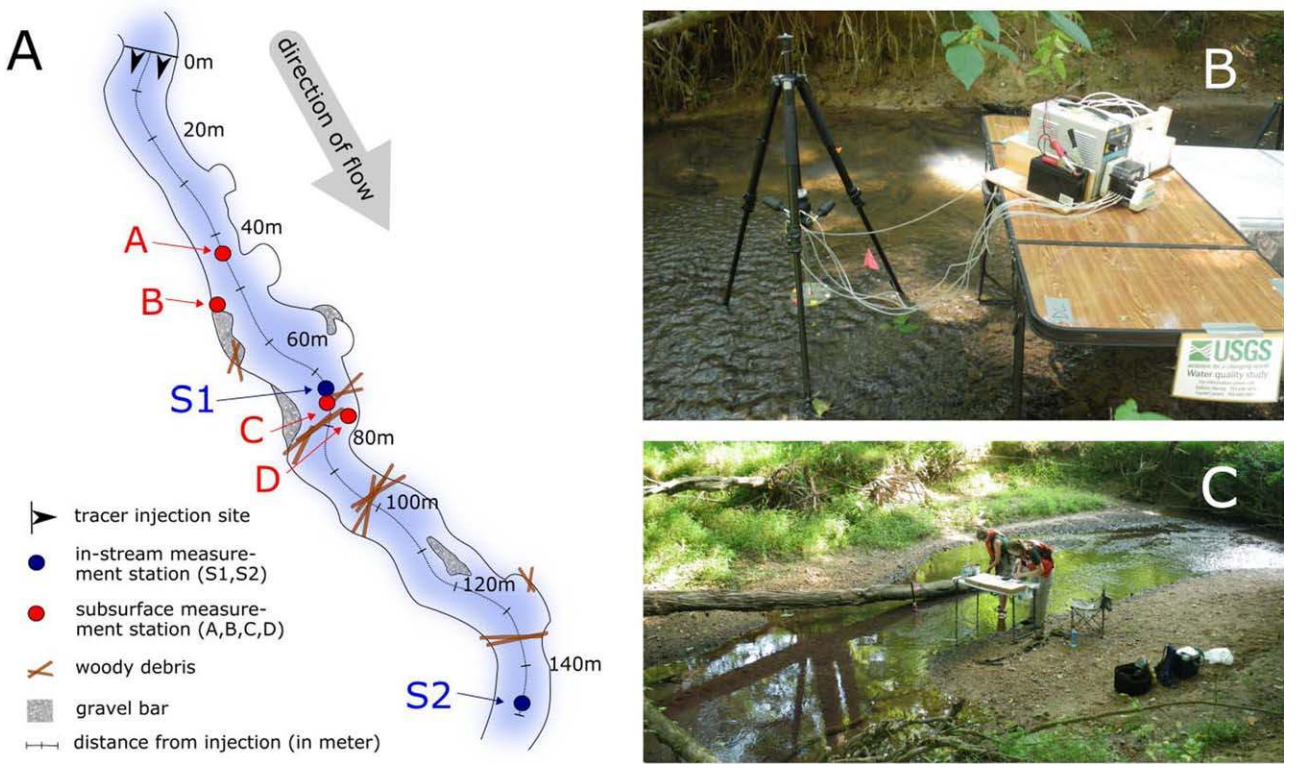

Figure 2. (a) Map of the study area, showing the locations of the injection as well as the different in-stream and subsurface measurement points. (b) Picture of the MINIPOINT setup: MINIPOINT sampler with tripod, peristaltic pump. (c) General overview of the stream with in-stream sampling point.

2.2. Sampling and Analysis of Field Data

The breakthrough curves (BTCs) of bromide, resazurin, and resorufin were recorded within the stream over the course of the experiment at two different locations, from here on referred to as S1 and S2. S1 was located 74.7 and S2 148.7 m downstream of the injection site (see Figure 2a). In-stream samples were collected with a peristaltic pump into syringe barrels fitted with polysulfone filters (0.2 μm pore size, 30 mm diameter, sealed disposable type) from which sample water was filtered directly into 22 mL sample bottles made of high-density polyethylene and capped with Polyseal tops. Bottles were stored cool out of direct sunlight. Sampling intervals ranged from 0.5 min during the rising and falling limbs of the breakthrough to 30 min under tracer-plateau conditions when tracer concentrations were relatively stable. Additionally, water samples from the shallow subsurface were simultaneously collected from several depths using a USGS MINIPOINT sampler as described by *Harvey and Fuller* [1998] and *Harvey et al*. [2013]. In total, four MINIPOINT samplers (labeled as A, B, C, and D in Figure 2a) were emplaced at distances of 44.0, 51.5, 77.4 and 79.7 m, respectively, from the injection site. MINIPOINT sampler A was emplaced in a 5 m long riffle, B in a lateral cavity of the stream near the right bank (oriented downstream), C in a channel thalweg between riffles, and D in a large pool near the left bank of the stream. MINIPOINT sampler B was omitted from the results because very little tracer entered the lateral cavity, leading to insufficient precision of the subsurface tracer concentrations to estimate reactive-transport parameters.

Each MINIPOINT sampler collected water samples of small volume (15 mL) at low rates (1.5 mL/min) from 1 cm slotted ports in 1/8 inch (nominal outside diameter) stainless-steel tubes situated approximately 2 cm above the bed and from four additional ports situated between 0.5 and 9 cm below the stream bed. Water samples were collected approximately every 10 min during the rising and falling limb of the tracer breakthrough in the stream, with longer intervals (30–40 min) between sampling during the period of stable conditions. The water samples were pumped through Masterflex size 13 tygon tubing and filtered inline by pumping through 0.2 μm pore size, 25 mm, *Pall* polysulfone filters and then directly into 22 mL high-density polyethylene (HDPE) scintillation vials supplied with HDPE polyseal caps.

Bromide concentrations of all samples were measured by ion chromatography (Dionex DX-120) with a Dionex AS-14 analytical column, AG-14 guard column, conductivity detector, 50 μL sample loop, and 3.4 mM sodium carbonate/L mM sodium bicarbonate eluent. Using this system, the detection limit of bromide is 15 μg/L. Concentrations of resazurin and resorufin were determined by fluorescence analysis with a Cary Eclipse Fluorescence Spectrophotometer (Agilent Technologies) at excitation/emission wavelengths of 602 nm/632 nm (resazurin) and 571 nm/584 nm (resorufin). The limit of quantification (LOQ) for resorufin is $<$0.05 nmol/L and $<$0.62 nmol/L for resazurin in DI water. Due to the overlap in spectra of the two compounds and the stronger fluorescence of resorufin, the LOQ of resazurin decreases if resorufin is present. The LOQ for both compounds is approximately five times greater in natural water than in DI water. All samples were kept cold in the dark until analysis, which was completed within a week of sampling. Due to a possible interference between the fluorescent signals of resazurin/resorufin and a fluorescent particle tracer that was coinjected with the dissolved tracers, the effect of the particles on the detection of resazurin was analyzed in the laboratory. The interference was found to be negligible at particle plateau concentrations because the particles (nominal 4 μm diameter) were nearly completely removed by filtering. In spite of filtering, however, some surface-water samples had high particle concentrations during periods of rapid sampling after the tracer injection stopped. For the subset of samples that had become contaminated with particles, the laboratory analysis revealed that the peak wavelength of the fluorescence spectrum of particles coincided with the analysis wavelengths of resorufin. For those samples, the resorufin concentrations were overestimated and the resazurin concentrations were slightly underestimated. The latter was caused by the interdependence of resazurin and resorufin concentrations in the matrix calculation used to determine concentrations from fluorescence signals [see *Lemke et al*., 2013b]. Therefore, extreme outliers of the calculated resazurin and resorufin concentrations fitting this pattern were removed. The number of outliers at any location and depth did not exceed 10% of the data points of the respective data set.

2.3. Modeling

In this section, we outline two models fitted to the data, Model I for reach-scale interpretation of surface water transport and subsurface exchange between the measurement stations S1 and S2, and Model II describing subsurface transport as a function of depth in the streambed using the MINIPOINT data sets A, C, and D. Both models were based on the one-dimensional advection-dispersion-reaction equation. Model I was a version of the transient storage model, which has often been applied to simulate conservative solute transport in streams [e.g., *Bencala and Walters*, 1983; *Zaramella et al*., 2003; *Runkel*, 2007]. It accounts for a single transient storage, ideally representing the hyporheic zone, which undergoes linear exchange with the stream [*Runkel*, 1998]. We amended the model with reaction terms for resazurin and resorufin that are only active in the hyporheic zone [see *Haggerty et al*., 2009; *Lemke et al*., 2013a, etc.]. The model cannot differentiate between a near surface benthic biolayer and the deeper hyporheic zone, because the model does not provide any spatial resolution of the hyporheic zone, but rather assumes a single, well-mixed hyporheic storage zone. Therefore, the reaction parameters are effective bulk parameters of the entire hyporheic zone.

Model II for the subsurface assumes one-dimensional, vertical transport underneath the stream, as it is commonly done for shallow hyporheic flow [e.g., *Harvey and Fuller*, 1998; *Bhaskar et al*., 2012]. Both models account for the compound-specific behavior of resazurin in the hyporheic zone including transformation of resazurin to resorufin in the hyporheic zone as well as retardation due to equilibrium sorption of resazurin and resorufin therein.

For the parameter estimation, we used the *DiffeRential Evolution Adaptive Metropolis* algorithm (DREAM(ZS)) [*Vrugt et al*., 2009; *Laloy and Vrugt*, 2012], a Markov chain Monte Carlo algorithm which provides full distributions of parameters conditioned on the measurements, and, thus, determined correlated parameter uncertainties. We constrained the parameters to be nonnegative and for the case of the retardation coefficients the lower limit was constrained to be 1. In a first optimization step, the parameters related to bromide and resazurin were jointly estimated. In a second optimization step, the previously determined parameters were sampled from their obtained distributions and parameters specific to resorufin only were estimated. This approach was chosen to decrease the ambiguity of the estimated parameter sets. To reduce autocorrelation between successively stored chain samples, we applied a thinning rate of 10 to the sets of estimated parameters. The goodness of the fits was determined by calculating the sum of squared residuals

normalized by the squared theoretical plateau concentration of each tracer. We refer to this quantity as normalized residual sum of squares, *nRSS* [-].

The analysis of in-stream data relies on comparing the change in tracer concentrations between sites S1 and S2 with the travel distance x [L] between these locations. The subsurface data were analyzed layer-wise, i.e., the concentrations recorded at the shallower depth were used as input signals, and those at the greater depth as output signals (e.g., layer 1 ranged from depth 0 to depth 1, layer 2 from depth 1 to depth 2, and so forth). In total, four depth layers were represented per location. In the analysis of the subsurface data, the travel distance Δz_k [L] is considered to be the vertical distance $d_{hz,k}$ [L] between the upper and lower MINIPOINT port of layer k (see Figure 1c). All concentrations reported from here on are corrected for background concentrations of the tracer compounds.

Calculating reaction rate coefficients from steady state concentrations by the approaches presented by *Harvey and Fuller* [1998], *Harvey et al*. [2013], and *González-Pinzón and Haggerty* [2013] was not feasible at most sampling depths because plateau concentrations were not reached at all subsurface measurement points. Also, dilution was significant and the sampling ended too early to capture the entire tail of the BTCs at these points. Instead, we fitted models to the time series of measured concentrations to obtain smooth simulated BTCs with complete tails and based our analysis on the moments and metrics of these simulated BTCs. We used temporal moment analysis, a common tool used to estimate central tendencies and model parameters in transport problems [e.g., *Kucera*, 1965; *Sardin et al*., 1991; *Harvey and Gorelick*, 1995], and details on their derivation can be found in the supporting information (Text S3).

Based on these model outcomes, we determined the depth and reactivity of the hyporheic zone as well as hyporheic residence times. Uncertainties of all metrics were calculated from an ensemble approach with 3125 realizations, by drawing parameters from their respective (thinned) distributions. Further details and derivations can be found in the supporting information.

2.3.1. Model I: In-Stream Transport With Hyporheic Exchange

Model I described the one-dimensional in-stream transport of the tracer compounds undergoing hyporheic exchange and hyporheic reactions (Figure 1b). Here, the hyporheic zone was considered a well-mixed transient-storage zone, characterized by a single concentration value for each compound at a given in-stream coordinate and time. As reach-based dilution was found to be insignificant between S1 and S2 (i.e., the conservative mass remained unchanged, see X^{br}_{reach} in Table 3), it was not included in the equations. The coupled governing equations were:

$$\frac{\partial c_i}{\partial t}+\frac{A_s}{A}R_i\frac{\partial c_{hz,i}}{\partial t}+v\frac{\partial c_i}{\partial x}-D\frac{\partial^2 c_i}{\partial x^2}=\frac{A_s}{A}r_{hz,i} \tag{1}$$

$$R_i\frac{\partial c_{hz,i}}{\partial t}=k\left(c_i-c_{hz,i}\right)+r_{hz,i} \tag{2}$$

subject to the following initial and boundary conditions:

$$c_i(x,t=0)=c_{hz,i}(x,t=0)=0\ \ \forall x \tag{3}$$

$$c_i(x=0,t)=c_{ini,i}(t);\ \ \lim_{x\to\infty}\frac{\partial^j c_i}{\partial x^j}=0\ \ \forall j\in\mathbb{N}_0. \tag{4}$$

in which c_i [ML^{-3}] denotes the in-stream concentration of compound i (0: bromide, 1: resazurin, 2: resorufin) and $c_{hz,i}$ [ML^{-3}] the corresponding concentration in the hyporheic zone; x [L] is the distance between S1 and S2; t [T] is time; the advective in-stream velocity is given by v [LT^{-1}]; D [L^2T^{-1}] is the longitudinal dispersion coefficient in the stream; $\frac{A_s}{A}$ [-] represents the ratio of the cross-sectional area of the storage zone A_s [L^2] to that of the stream A [L^2]; k [T^{-1}] is the first-order mass transfer rate coefficient between the stream and the transient storage zone. Our reference volume of the mass-transfer coefficient was that of the transient storage zone, whereas in other works [e.g., *Bencala and Walters*, 1983] the reference volume typically is that of the stream. Conversion implies that our coefficient k equals $\frac{A}{A_s}\alpha$ in *Bencala and Walters* [1983]. Furthermore, R_i [-] represents the retardation factor of compound i in the hyporheic zone, assuming linear sorption at local equilibrium; and $r_{hz,i}$ [$ML^{-3}T^{-1}$] is the reaction rate of compound i in the hyporheic zone. Bromide is considered an ideal tracer that neither sorbs nor undergoes transformations, therefore

$$R_0 = 1 \text{ and } r_{hz,0} = 0$$

whereas both resazurin and resorufin may sorb within the streambed ($R_1 \geq 1;\ R_2 \geq 1$). The chemical transformations of resazurin and resorufin within the hyporheic zone were assumed to follow linear reaction kinetics, resulting in the following reaction rates:

$$r_{hz,1} = -\lambda_1 c_{hz,1} \tag{5}$$

$$r_{hz,2} = \lambda_{12} c_{hz,1} - \lambda_2 c_{hz,2} \tag{6}$$

in which λ_1 [T^{-1}] is the rate coefficient of total resazurin transformation; λ_{12} [T^{-1}] is the rate coefficient describing the transformation of resazurin to resorufin; and λ_2 [T^{-1}] is the rate coefficient of resorufin transformation. The transformation of resazurin to resorufin cannot exceed the total transformation of resazurin, thus requiring $\lambda_{12} \leq \lambda_1$.

The equations above were analytically solved in the Laplace domain and back-transformed numerically [*Hollenbeck*, 1998]. A detailed derivation is given in the supporting information (Text S1).

As presented above, the transient-storage model assumed a perfectly mixed hyporheic zone. As there is no mixed reactor in the subsurface in reality, the physical interpretation of fitted parameters may thus be misleading. The set of equations presented above, however, can also be interpreted in a different way [e.g., *Wörman*, 1998; *Liao and Cirpka*, 2011; *Lemke et al*., 2013a]. Based on a mass balance of the solutes in the stream alone, with a partial retention of the solutes caused by hyporheic exchange, the stream-transport equations for bromide and resazurin (equations (1) and (2)) can be represented as:

$$\frac{\partial c_i}{\partial t} + v\frac{\partial c_i}{\partial x} - D\frac{\partial^2 c_i}{\partial x^2} = q_{he,reach}\left(\int_0^\infty \frac{k}{R_i}\exp\left(-\left(\frac{k}{R_i}+\lambda_i\right)\tau\right)c_i(t-\tau)d\tau - c_i(t)\right) \tag{7}$$

in which τ [T] is the time that a solute particle has spent in the hyporheic zone when coming back into the stream, and the hyporheic exchange rate $q_{he,reach}$ [T^{-1}] can be interpreted as the fraction of stream water undergoing hyporheic exchange per time [see *Liao and Cirpka*, 2011 for a more detailed explanation]. $q_{he,reach}$ in equation (7) was computed from the coefficients of the previous formulation of Model I by:

$$q_{he,reach} = \frac{A_s}{A}k. \tag{8}$$

Equations (1) and (7) merely differ in the conceptualization of the hyporheic zone. Whereas equation (1) conceptualizes a defined size of the storage zone, equation (7) parameterizes the effects of hyporheic exchange on in-stream transport by an exchange coefficient $q_{he,reach}$ and the distribution of hyporheic travel times, here assumed to follow the exponential distribution $k\exp(-k\tau)$. Sorption within the hyporheic zone is expressed as retardation of the travel-time distribution, and first-order transformation by the exponential loss of solute mass as function of time spent in the hyporheic zone.

2.3.2. Model II: Transport Within the Hyporheic Zone

For comparability, Model II for reactive transport in the subsurface was also based on the one-dimensional advection-dispersion-reaction equation, adapted for admixture of groundwater (Figure 1c):

$$\frac{\partial c_{0,hz}}{\partial t} + v_z\frac{\partial c_{0,hz}}{\partial z} - D_z\frac{\partial^2 c_{0,hz}}{\partial z^2} = q_{in}\left(c_{0,GW} - c_{0,hz}\right) \tag{9}$$

$$R_{1z}\frac{\partial c_{1,hz}}{\partial t} + v_z\frac{\partial c_{1,hz}}{\partial z} - D_z\frac{\partial^2 c_{1,hz}}{\partial z^2} = -\lambda_1 c_{1,hz} + q_{in}\left(c_{1,GW} - c_{1,hz}\right) \tag{10}$$

$$R_{2z}\frac{\partial c_{2,hz}}{\partial t} + v_z\frac{\partial c_{2,hz}}{\partial z} - D_z\frac{\partial^2 c_{2,hz}}{\partial z^2} = -\lambda_2 c_{2,hz} + \lambda_{12} c_{1,hz} + q_{in}\left(c_{2,GW} - c_{2,hz}\right) \tag{11}$$

in which z [L] denotes the spatial coordinate along the hyporheic flow path, simplified as depth; q_{in} [T^{-1}] is a rate coefficient accounting for mixing with groundwater, which can be interpreted as the groundwater discharge added to the river-borne water per volume of pore space. $c_{i,GW}$ [ML^{-3}] is the concentration of compound i in groundwater—note that in the present application $c_{i,GW} = 0$ for all compounds, because the admixed groundwater does not contain any tracer compound added into the stream. The net effect of mixing with groundwater is therefore dilution, which is mathematically identical to first-order transformation

with the rate coefficient q_{in}. In reality, mixing with groundwater is affected by complicated three-dimensional flow fields that cannot be resolved in a 1-D model considering only vertical transport. Thus, in our model, groundwater dilution is treated as lateral inflow, affecting concentrations at every depth section of the hyporheic zone and not just the lowest layer. This dilution term acts to the same extent on the conservative compound bromide as on the reactive compound and its product, whereas the effects of reaction of resazurin and resorufin (i.e., λ_1 and λ_2, respectively) are exclusive to the non-conservative compounds. All other terms are as previously defined for Model I, but for vertical subsurface transport. Because z is a depth coordinate, the transport parameters v_z and D_z should be referred to as apparent parameters of vertical transport.

The equations of hyporheic transport were solved between two consecutive layers (i.e., shallower BTCs become fixed-concentration upstream boundary conditions). To solve these equations, we assumed a semi-infinite domain and solved the system of equations analytically in the Laplace domain, followed by numerical back-transformation into the time domain. A detailed derivation of the above equations is given in the supporting information (Text S2). All parameters are estimated as function of depth z, meaning that they were allowed to differ between the different depth compartments. A depth compartment is defined here as the depth section between two consecutive MINIPOINT ports.

Model II only simulates the water entering the hyporheic zone and makes no assumptions about the fate of the water remaining in the channel. However, the exchange rate q_{he} [T^{-1}] between stream and hyporheic zone was evaluated from the topmost layer, analogous to the one obtained from the reach-scale approach (equation (8)):

$$q_{he} = \frac{v_z}{\theta w_{hz}} \tag{12}$$

in which θ [-] denotes the porosity of the streambed, and w_{hz} [L] is the width of the hyporheic zone (approximated by the measured active channel width).

2.4. Comparison of Surface and Subsurface Results

A direct interpretation of model parameters is typically regarded with skepticism, because assessing the validity of the obtained parameters is not straightforward, particularly in light of noisy data and missing tracer tails in conjunction with BTCs not reaching steady state (plateau) values. As a result it is difficult to estimate tracer recovery and the appropriate hyporheic residence time directly from the data. The selection of the residence time distribution, however, influences the estimated model parameters. To improve our interpretation, we instead used the model to generate smooth, complete BTCs—the validity of which is easily assessed by comparing the measured and simulated concentrations. We then based our interpretation on temporal moments of these fitted BTCs or, to be more explicit, on BTCs that would be obtained if the stream signal was a perfect Dirac delta pulse. We reasoned that by fitting a model, the truncated BTCs could be extrapolated in a manner that was consistent with the observed data. The measured part of the BTC did not need to approach the base value again, but it did need to include a peak and at least the beginning of the falling limb, in order to obtain reliable model parameters and temporal moments. Of course, if the true tracer BTCs exhibited a contribution with a rapid drop and a very elongated tail with low values we would have missed that, but, very likely, we would have missed it also with extended sampling as low values tend to disappear in the noise of base line, which can lead to errors in tracer recovery.

2.4.1. Analysis of Tracer Recovery

Tracer recovery in the stream was evaluated from ratios of plateau concentrations $c_{plateau}$ at the upstream and downstream locations, because stable plateau concentrations were reached in the stream at both measurement locations:

$$X_{reach} = \frac{c_{plateau}(\mathrm{S2})}{c_{plateau}(\mathrm{S1})}. \tag{13}$$

For subsurface data, a decrease in reactive tracer concentrations with depth can be caused by both dilution (through mixing of river-borne water with groundwater) and transformation, whereas the conservative tracer is only affected by dilution. Dilution, reaction, and dispersion not only influence concentrations, but also affect the propagation velocity of concentration fronts, termed celerity. Thus, the celerity v_* is usually larger

than the advective velocity v, because it accounts for the effects of dilution and transformation. For the conservative tracer bromide, the celerity v_{0*} [LT^{-1}] was calculated as follows:

$$v_{0*} = \sqrt{v^2 + 4Dq_{in}} \tag{14}$$

whereas for the reactive tracer resazurin, the celerity v_{1*} [LT^{-1}] became:

$$v_{1*} = \sqrt{v^2 + 4D(q_{in} + \lambda_1)}. \tag{15}$$

A derivation of equations (14) and (15) is given in the supporting information (Text S3).

We identified the fraction of river-borne water in the hyporheic zone at depth z as the recovery $X_{rec}^{br}(z)$ [-] of the conservative tracer. It is related to the transport coefficients of the subsurface-transport model by:

$$X_{rec}^{br}(z) = \exp\left(-\int_0^z \frac{v_{0*} - v}{2D}\, d\zeta\right) = \exp\left(-\int_0^z \frac{2q_{in}}{v + \sqrt{v^2 + 4Dq_{in}}}\, d\zeta\right) \tag{16}$$

which can be derived from analyzing the zeroth temporal-moment of the conservative tracer (see supporting information Text S3). The integral with the variable of integration ζ in equation (16) and in following expressions was determined from fitted constant transport parameters for each layer. In steady state transport, the recovery $X_{rec}^{br}(z)$ would be the concentration of the conservative tracer at depth z divided by the concentration in the river.

The recovery of the conservative tracer in the subsurface profile was used to determine an equivalent depth $\tilde{d}_{hz}$ [L] of the hyporheic zone at the different MINIPOINT sampler locations. For this purpose, values of the tracer recovery $X_{rec}^{br}(z)$ at sampling depths were exponentially interpolated layer-wise and also exponentially extrapolated. Then, the equivalent depth $\tilde{d}_{hz}$ [L] of the hyporheic zone is the depth-integral of the recovery profile:

$$\tilde{d}_{hz} = \int_{z=0}^{\infty} X_{rec}^{br}(z)\, dz. \tag{17}$$

This equivalent depth quantifies the theoretical extent of the hyporheic zone if it contained only stream water. It is necessary to quantify the hyporheic depth in this way instead of using other definitions (i.e., $\geq$10% surface water recovery, as defined by *Triska et al.* [1989]) to obtain comparability to the size of the transient-storage zone assumed by the in-stream-transport model (i.e., A_s), because the transient-storage model does not account for mixing with groundwater within the transient-storage zone, but assumes that the storage zone only contains river-borne water.

We compared the equivalent depth d_{hz} to the apparent depth of the hyporheic zone $\tilde{d}_{hz,reach}$ [L] calculated from the relative hyporheic storage area of the reach-scale transient storage Model I:

$$\tilde{d}_{hz,reach} = \frac{A_s}{A}\, A_{meas}\, \frac{1}{w_{hz}\theta} \tag{18}$$

In this, the measured cross-sectional area of the stream, A_{meas} [L^2], is multiplied by the relative storage zone size to estimate the full hyporheic zone depth in sediment.

While the analysis of the bromide profiles in the subsurface provided information on mixing with groundwater and the extent of the hyporheic zone, the depth profiles of the reactive tracer gave information about subsurface reactivity. We directly assessed the reactivity using an estimated rate coefficient λ_{Raz} [T^{-1}] describing total resazurin transformation. We also computed the recovery $X_{rec}^{raz}(z)$ [-] of resazurin as function of depth, which can be interpreted as the steady-state plateau concentration of resazurin at depth z normalized by the river concentration if the latter was constant. To do so, we repeat the operation of equation (15) using the celerity v_{1*} of resazurin (equation (14)) rather than the one of bromide, v_{0*}:

$$X_{rec}^{raz}(z) = \exp\left(-\int_0^z \frac{v_{1*} - v}{2D}\, d\zeta\right) = \exp\left(-\int_0^z \frac{2(q_{in} + \lambda_1)}{v + \sqrt{v^2 + 4D(q_{in} + \lambda_1)}}\, d\zeta\right). \tag{19}$$

We used the recoveries of the conservative and reactive tracers at paired observation depths to compute a reaction factor f_{reac} [-] that expressed the relative mass loss of the reactive tracer occurring over the depth difference Δz corrected for the effect of dilution:

$$f_{reac}(z+\Delta z)=1-\frac{X_{rec}^{raz}(z+\Delta z)}{X_{rec}^{raz}(z)}\cdot\frac{X_{rec}^{br}(z)}{X_{rec}^{br}(z+\Delta z)}. \quad (20)$$

In analogy to the equivalent depth $\tilde{d}_{hz}$ of the hyporheic zone, defined in equation (17), we computed a penetration depth $\tilde{d}_{raz}$ [L] of resazurin by considering the depth-integral of the resazurin recovery:

$$\tilde{d}_{raz}=\int_0^\infty X_{rec}^{raz}(z)dz. \quad (21)$$

$\tilde{d}_{raz}$ is a metric of the depth-distribution of resazurin and quantifies the reactive part of the hyporheic zone and therefore the part of the subsurface with particularly high metabolic activity. There is no equivalence in the transient-storage model for reach-scale transport, as it assumes that the hyporheic zone is perfectly mixed, implying that all constituents reach the same depth.

We compared the total normalized steady state mass of resazurin stored in the hyporheic zone to that of bromide (in which normalization is done with the in-stream concentration). Toward that end, we divided the penetration depth $\tilde{d}_{raz}$ of resazurin by the equivalent depth $\tilde{d}_{hz}$ of the hyporheic zone, resulting in a reaction factor f_{reac}^{tot} [-] for the entire hyporheic zone:

$$f_{reac}^{tot}=1-\frac{\tilde{d}_{raz}}{\tilde{d}_{hz}}. \quad (22)$$

In the reach-scale transient-storage model, the same ratio of masses in the hyporheic zone is the ratio of steady state concentrations in the well-mixed transient storage zone:

$$f_{reac,reach}^{tot}=1-\frac{k}{k+\lambda_{Raz}}=\frac{\lambda_{Raz}}{k+\lambda_{Raz}}. \quad (23)$$

To complete the analysis, for the reach-scale transport analysis we computed the recovery $X_{rec,reach}^{raz}(x)$ [-] of the reactive tracer in the stream using a derivation that considered the steady state solution of the transient-storage model:

$$X_{rec,reach}^{raz}(x)=\exp\left(-\frac{2\lambda_{eff}}{v+\sqrt{v^2+4D\lambda_{eff}}}\,x\right) \quad (24)$$

with the effective first-order transformation coefficient λ_{eff} [T^{-1}] for reach-scale transport:

$$\lambda_{eff}=\frac{A_s}{A}\cdot\frac{k\lambda_{Raz}}{k+\lambda_{Raz}}. \quad (25)$$

That approach was analogous to the calculation of tracer recovery we made for the subsurface. Details are given in the supporting information (Text S4).

2.4.2. Analysis of Hyporheic Water Ages

The mean hyporheic transport time was assessed for subsurface BTCs using an analysis of first temporal moments of the conservative tracer (see supporting information Text S3), which yielded the mean hyporheic water age $\tau(z)$ [T] as a function of depth:

$$\tau(z)=\int_0^z\frac{1}{v_{0^*}(\zeta)}d\zeta. \quad (26)$$

where $\tau(z)$ corresponded to the center of mass of a conservative-tracer BTC if the concentration in the river was a perfect pulse.

The mean age of the stream water in the entire hyporheic zone was estimated as the recovery-weighted average of $\tau(z)$:

$$\tilde{\tau}_{hz}=\frac{1}{\tilde{d}_{hz}}\int_0^\infty\tau(z)X_{rec}^{br}(z)\;dz. \quad (27)$$

We compare this value to the reach-scale apparent mean hyporheic water age $\tilde{\tau}_{hz,reach}$ [T] evaluated by the fitted transient-storage model, which was estimated as the inverse of the first-order exchange coefficient k [T^{-1}]:

$$\tilde{\tau}_{hz,reach} = \frac{1}{k}. \tag{28}$$

This residence time applies to the conservative and the reactive tracer, due to the assumption of a perfectly mixed single storage zone of the transient storage model. From the subsurface data, on the other hand, an apparent age $\tau_{raz}(z)$ [T] of the metabolically active resazurin can be calculated in analogy to equation (26):

$$\tau_{raz}(z) = \int_0^z \frac{R_1}{v_{1*}(\zeta)} d\zeta. \tag{29}$$

2.4.3. Analysis of Solute Spreading

We furthermore analyze the spreading of the solute time series, for both hyporheic and in-stream transport, which was calculated for the hyporheic zone as:

$$\sigma_\tau^2(z) = \int_0^z \frac{2D}{v_{0*}^3} d\zeta. \tag{30}$$

For the reach-scale approach, the mean in-stream arrival times were obtained from temporal moments of the BTCs using:

$$\tau_{reach} = \frac{\mu_1(t)}{\mu_0(t)} \tag{31}$$

with the zeroth temporal moment $\mu_0(t) = \int_0^\infty c(t)\ dt$ and the first temporal moment $\mu_1(t) = \int_0^\infty c\ t\ dt$. The travel time between the stations S1 and S2 was calculated as the difference between the arrival times and the spreading of the BTC (i.e., the variance of in-stream travel times) was calculated as follows:

$$\sigma_{\tau,reach}^2 = 2\left(\frac{D}{v^2}\left(\frac{A_s}{A}+1\right)^2 + \frac{A_s}{Ak}\right)\frac{x}{v}. \tag{32}$$

The square root of the equations (30) and (32) denote the standard deviations and thus define the range of arrival times and water ages, i.e., the solute spreading.

3. Results and Discussion

In this section we first present the stream characteristics and all of the in-stream results, then we focus on the outcomes from the analysis of the subsurface data, and we close with a comparison across scales. The characteristic parameters obtained from in-stream data were compared to subsurface parameters to analyze if in-stream tracer tests are able to provide good information on the depth of the hyporheic zone, hyporheic water ages, and the distribution and rates of reactivity in the hyporheic zone.

3.1. Stream Characteristics and In-Stream Results

The fit between simulated and measured in-stream concentrations (Figure 3) was generally good as indicated by the low magnitude of the normalized residual sum of squares $nRSS_{br}$ and $nRSS_{raz}$ (Table 1), and all obtained parameters lay in the expected ranges (i.e., similar to values obtained, e.g., by *Haggerty et al.* [2009]; *Lemke et al.* [2013a]; and *Liao et al.* [2013]). The quality of the fit of the tailing and thus the longer residence times were represented less accurately because sampling was stopped at the beginning of the spate. Although we acknowledge that previous data sets have shown that hyporheic residence time distributions may be better fitted with broader than exponential tailing, i.e., power-law or nonparametric residence time distributions [i.e., *Wörman et al.*, 2002; *Gooseff et al.*, 2003; *Liao and Cirpka*, 2011], our simple transient storage model with a single storage zone with an exponential residence time distribution was able to capture the main processes observed. Thus, the application of a more complex model would not have been justified for our data.

The full mass of bromide found at S1 was recovered at S2 and therefore dilution was insignificant along the reach. Also, the transformation of resazurin along the reach resulted in a recovery of only 88% of the mass found at S1 (see Table 1). Arrival times between bromide and resazurin did not differ greatly (see vertical lines in Figure 3) and the BTCs generally exhibited a low amount of solute spreading ($\sigma_\tau = 20.0 \pm 6.4$ min).

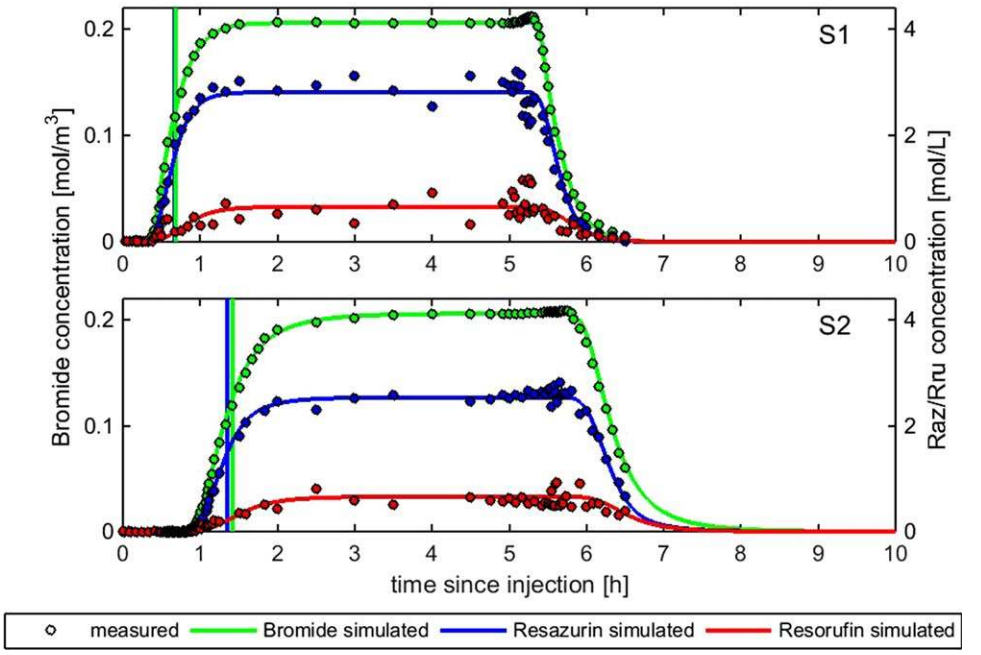

Figure 3. Measured and simulated in-stream tracer breakthroughs for Difficult Run at stream sites S1 and S2 with tracer concentrations. Points indicate measured concentrations and lines show simulated concentrations for the joint fit of bromide, resazurin, and resorufin. Vertical lines indicate the mean arrival times of the rising limbs for bromide and resazurin as calculated from moments of the BTCs.

The measured cross-sectional area of the channel, A_{meas}, was approximately 22% larger than the one calculated from streamflow discharge, distance, and travel time (Table 1). This indicates that tracer transport primarily occurred through a cross-sectional area that was smaller than the observable active channel, which already excluded areas of still or recirculating flow. The advective in-stream velocities v obtained from

Table 1. Results From the Stream Survey, Calculated Characteristics, Metrics, and Estimated Parameters for the In-Stream Sections From Model Fitting[a]

Parameter	Description	Units	Survey	Calculated	Model Fit
θ	Porosity		0.39		
x	Longitudinal distance between S1 and S2	(m)	74.0		
τ	Conservative in-stream travel time	(min)		44.6	
σ_τ	Conservative in-stream solute spreading	(min)		20.1 ± 6.4	
X^{br}_{reach}	Bromide recovery			1.00	
X^{raz}_{reach}	Resazurin recovery			0.88	
v	Advective velocity	(m/s)		2.8e-2[b]	3.3e-2 ± 1.6e-4
Q	Discharge	(m^3/s)		0.027	
w_{hz}	Width of the hyporheic zone	(m)	5.57[c]		
A_{meas}, A	Channel cross-sectional area	(m^2)	1.26[c]	0.98[d]	
D	Dispersion coefficient	(m^2/s)			5.3e-2 ± 2.2e-3
k	First-order mass transfer rate coefficient	(1/s)			6.0e-4 ± 2.5e-5
A_s/A	Relative size of the storage zone				1.9e-1 ± 4.9e.3
R_1	Retardation factor of resazurin				1.45 ± 8.7e-2
λ_1	Total transformation coefficient of resazurin	(1/s)			4.0e-4 ± 3.5e-5
R_2	Retardation factor of resorufin				1.36 ± 1.5e-1
λ_{12}	Resazurin to resorufin transformation coefficient	(1/s)			3.2e-4 ± 1.8e-5
λ_2	Transformation coefficient of resorufin	(1/s)			7.6e-4 ± 1.2e-4
$nRSS_{br}$	Normalized RSS for bromide				1.8e-2
$nRSS_{raz}$	Normalized RSS for resazurin				7.5e-2
$nRSS_{rru}$	Normalized RSS for resorufin				2.51

[a]The modal value of each obtained parameter distribution is given with its respective standard deviation.
[b]Calculated as $v = x/\tau$.
[c]Assumed to be identical to the measured width of the active channel ignoring zones with still or recirculating flow, denoted A_{meas} in equation (18).
[d]Calculated as $A = Q\tau/x$.

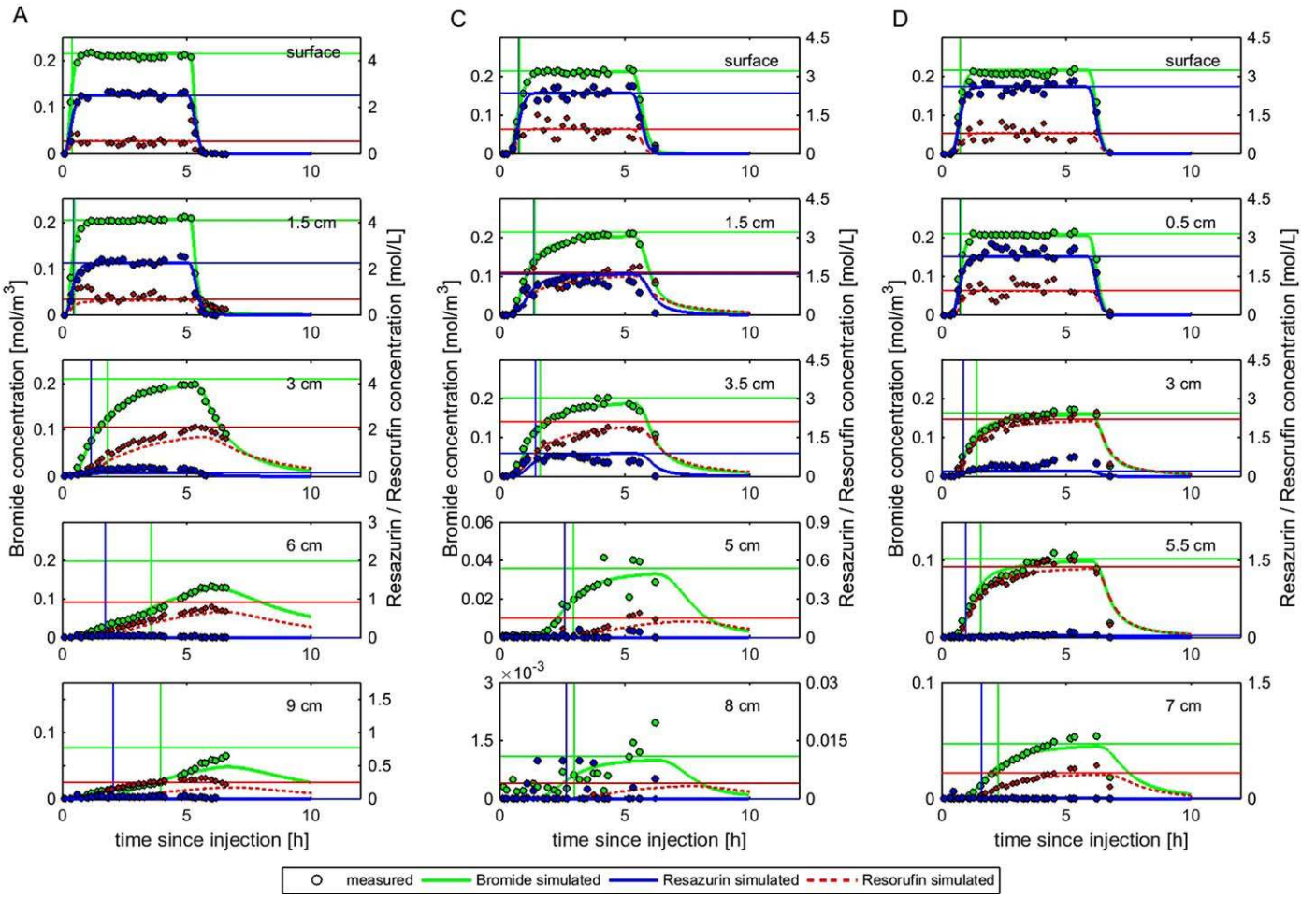

Figure 4. Measured (points) and fitted (lines) subsurface data for A (first column), C (second column) and D (third column). Horizontal lines indicate the theoretical plateau concentrations of the different compounds that would be obtained for a longer constant injection. The vertical lines indicate mean arrival times of the rising limb (obtained by subtracting half the injection duration from first temporal moments of the complete, simulated BTCs).

calculations and inverse modeling agree, and the uncertainties of all parameters related to the conservative and reactive tracer are relatively low. However, because the fitted rate coefficients of resazurin-to-resorufin transformation, λ_{12}, and transformation of resorufin, λ_2, are usually highly correlated (visible, i.e., in the correlation plot found in the supporting information Figures S1–S13), we chose to interpret hyporheic processes based on the transformation of resazurin alone. Resorufin measurements, on the other hand, are used to confirm the validity of the estimated parameters, by verifying that the measured resorufin curves can be reproduced with the estimated parameters.

3.2. Subsurface Results

The goodness of fit of the simulated BTCs decreased with depth in the hyporheic zone (Figure 4), but the generally good fits indicate the validity of the model used. All obtained parameters also lay in the expected ranges (see supporting information Table S1–S3). However, it should be noted here that the amount of missing part of the tails of the measured BTCs was greater with depth, and thus the quality of simulations decreased with depth and all calculations became less certain at greater depths.

The concentrations of bromide and resazurin decreased with depth, leading to lower theoretical plateau concentrations in deeper layers. Consequently, the concentrations of resorufin increased slightly until the third or fourth depths. Furthermore, the bromide BTCs became increasingly wider with depth to the point that plateau values could not be reached with the given injection time. Resazurin curves showed less spreading and tailing than bromide curves due to its transformation, which led to earlier mean arrival times for this compound than for bromide (see vertical lines in Figure 4). The spreading in the BTCs reveal an

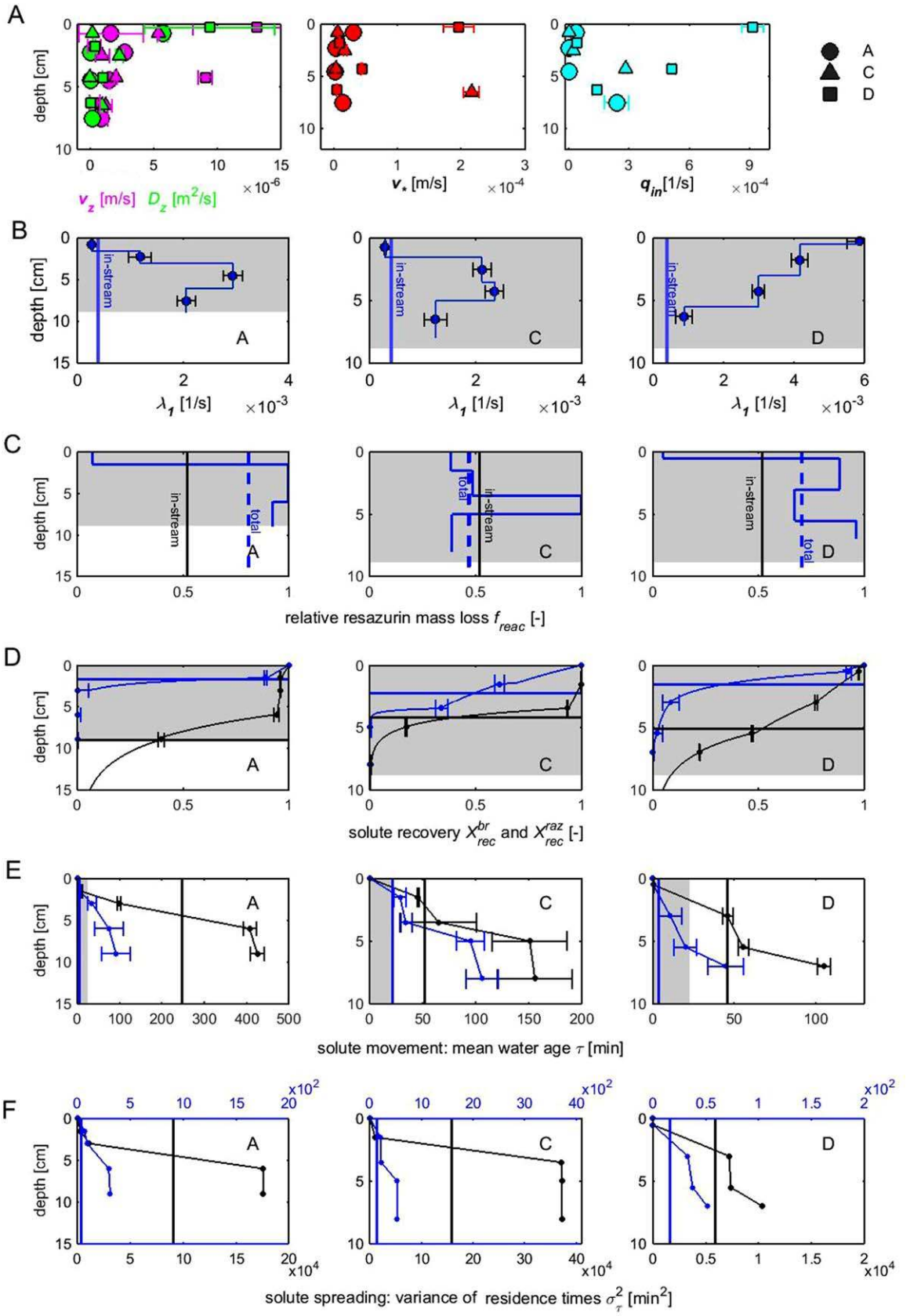
A
depth [cm]
v_z [m/s] D_z [m^2/s]
$\times 10^{-6}$
v_* [m/s]
$\times 10^{-4}$
q_{in}[1/s]
$\times 10^{-4}$
A
C
D
B
in-stream
λ_1 [1/s]
$\times 10^{-3}$
C
in-stream
total
relative resazurin mass loss f_{reac} [-]
D
solute recovery X_{rec}^{br} and X_{rec}^{raz} [-]
E
solute movement: mean water age τ [min]
F
$\times 10^2$
$\times 10^4$
solute spreading: variance of residence times σ_τ^2 [min^2]

Figure 5.

increasing distribution of mean water ages with depth (Figures 5e and 5f). For bromide, the decrease in concentration with depth was caused by mixing with tracer-free groundwater. For resazurin, the concentration decrease was even stronger, because it underwent transformation in addition to dilution. For resorufin, the concentration only decreased once the effect of dilution became stronger than production. The decrease in tracer concentrations with depth was described well by the calculated recovery rates (see Table 2 and Figure 5d).

The relative mass loss of resazurin f_{reac} due to transformation was generally higher in the upper layers of the hyporheic zone than in the lower layers (see Figure 5c), leading to a fast disappearance of the reactive tracer with depth (see Figure 5d). The relative reactive mass loss f_{reac} (Figure 5c) expresses which fraction of the reactive tracer is lost by reaction, corrected for dilution and regardless of the time needed, whereas the reaction rate constants λ_1 [T^{-1}] (Figure 5b) is a reaction rate [$ML^{-3}T^{-1}$] scaled by the concentration. The two profiles differ because the time increments in the various layers differs.

This is in agreement with the concept of the benthic biolayer, which postulates that higher transformation potential and more pronounced transformation processes occur not only at the stream-sediment interface, but throughout the upper, highly reactive layer of the hyporheic zone. This is consistent with studies recording strong metabolic activity and steep gradients in the upper layer of the sediment [e.g., *Arnon et al.*, 2013]. Interestingly, however, only at MINIPOINT sampler D did we observe the highest transformation coefficient λ_1 directly at the top of the streambed, whereas for both A and C the layer of highest reactivity was located at slightly greater depths. These differences between locations are likely higher than those between layers and may be due to different processes at the sampling locations. While D was positioned in a pool towards the bank of the stream, both A and C had been placed in the channel center. Possibly, the increased turbulence in the channel led to a disturbance of the upper sediment, whereas calmer conditions in the pool created favorable conditions for higher metabolic activity at the stream-sediment interface.

Figure 5a illustrates the decrease of the apparent velocity v_z and the apparent dispersion coefficient D_z with depth. Due to the model-implicit assumption of vertical flow paths, these values should not be confused with actual parameter values observed along the true (unknown) flow paths, which are reduced here to their vertical component. Nevertheless, they followed an expected decrease with depth. For the celerity v_{0*} this decreasing trend was less pronounced, due to the adjustment for increasing discharge q_{in}, which is also shown in the same figure.

For MINIPOINT profiles C and D, the tracer recovery X_{rec}^{br} at the deepest ports amounted to less than 20%, suggesting large influence of groundwater at great depths. Therefore, the sampled profiles span the whole range from stream water dominated to groundwater dominated BTCs, yielding informative metrics of transport and reactivity. In contrast, for the MINIPOINT profile A the subsurface sampling did not reach deep enough to get close to the depth where groundwater dominates. Instead, the recovery trend toward greater depths had to be approximated, yielding less informative results.

3.3. Comparison of the Results

So far, in-stream and subsurface results were discussed separately. Here we compare reach-scale and subsurface parameters which allows for an increased understanding of the different information gained from the two approaches.

The transformation rate coefficients λ_1 determined for the hyporheic zone by the reach-scale analysis were lower than those determined directly in the subsurface (Figure 5b), particularly at the shallower depths. This

Figure 5. (a) Depth-wise illustration of the estimated vertical parameters obtained from model fitting of the subsurface data for profiles A (circles), C (triangles), and D (squares) of apparent velocity v (m/s), celerity v_{0^*} (m/s) according to equation (14), apparent dispersion coefficient D (m^2/s) and discharge rate coefficient q_{in} (1/s); (b) first-order transformation coefficient λ_1 [T^{-1}] of resazurin; the vertical line represent the equivalent estimated reach-scale processing rate coefficient; (c) relative resazurin mass loss f_{reac} according to equation (20), total mass loss according to equation (22) (blue vertical line), and in-stream mass loss according to equation (23) (black vertical line); (d) calculated recovery rates for the conservative tracer X_{rec}^{br} according to equation (16) (black) and reactive tracer X_{rec}^{raz} according to equation (19) (blue) with the subsurface estimated hyporheic zone depth $\bar{d}_{hz}$ according to equation (17) (horizontal black line) and in-stream tracer estimated hyporheic zone depth $\bar{d}_{hz,reach}$ according to equation (18) (grey areas) and the reactive depth $\bar{d}_{raz}$ according to equation (21) (blue line); (e) mean water age τ as calculated for the conservative tracer according to equation (26) (black markers) and the reactive tracer according to equation (29) (blue markers). The average age for the location is given by the vertical black line, the patched area indicates the mean water age as calculated from the reach-scale fit according to equation (28) (13 min); (f) solute spreading σ_{tau}^2 with depth according to equation (30).

Table 2. Lengths of the Hyporheic Depth Layers Δz, Layer-Wise Calculated Mean Water Ages $\Delta\tau$, Cumulative Mean Water Age at the Bottom of the Given Layer, $\tau_{hz}(z_{bot})$, Layer-Wise Reaction Rates of Resazurin, f_{reac}, and Fractions of River-Borne Bromide and Resazurin Recovery at the Different Subsurface Depths, $X^{br}_{rec}(z_{bot})$ and $X^{raz}_{rec}(z_{bot})$

	A (Channel Center)				C (Channel Center)				D (Pool)			
	Sec 1	Sec 2	Sec 3	Sec 4	Sec 1	Sec 2	Sec 3	Sec 4	Sec 1	Sec 2	Sec 3	Sec 4
Δz (cm)	1.5	1.5	3	3	1.5	2	1.5	3	0.5	2.5	2.5	1.5
$\Delta\tau$ (min)	6.8 ± 4.5	91.3 ± 0.4	306.7 ± 15.4	14.0 ± 8.2	45.5 ± 0.8	13.4 ± 36.6	89.6 ± 2.7	2.2 ± 8.2	0.4 ± 0.3	45.5 ± 3.2	9.1 ± 0.4	47.5 ± 2.4
$\tau_{hz}(z_{bot})$(min)	6.8 ± 4.5	98.8 ± 4.4	406.9 ± 15.4	425.4 ± 16.6	45.5 ± 0.8	64.9 ± 35.7	151.2 ± 35.2	156.1 ± 35.3	0.4 ± 0.3	46.0 ± 3.2	55.5 ± 3.2	105.0 ± 4.0
f_{reac}	0.07 ± 5e-3	0.996 ± 6e-2	0.998 ± 5.4e-2	0.92 ± 5.4e-2	0.38 ± 2e-2	0.49 ± 3e-2	0.998 ± 6e-2	0.39 ± 4e-2	0.05 ± 1e-2	0.88 ± 5e-2	0.67 ± 4e-2	0.96 ± 6e-2
$X^{br}_{rec}(z_{bot})$	0.96 ± 2e-3	0.96 ± 2e-3	0.94 ± 1.4e-2	0.40 ± 1.4e-2	1.00 ± 2e-3	0.93 ±4e-3	0.17 ± 3e-2	0.01 ± 4e-4	0.97 ± 2e-3	0.77 ± 5e-3	0.47 ± 3e-3	0.22 ± 3e-3
$X^{raz}_{rec}(z_{bot})$	0.89 ± 6e-3	3.5e-3 ± 5e-2	4.7e-4 ± 1.4e-2	1.2e-4 ± 3.4e-3	0.61 ± 2e-2	0.34 ± 3e-3	2.7e-4 ± 8e-3	6.4e-6 ± 2e-4	0.93 ± 1e-2	0.08 ± 4e-2	0.02 ± 2e-2	2.1e-4 ± 6e-3

was similar for the total mass loss f^{tot}_{reac} (Table 3), i.e., while approximately 50% of the resazurin entering the hyporheic zone was lost according to the in-stream results, up to 80% mass loss was detected along the subsurface flow paths, leading to much lower resazurin concentrations at the deeper subsurface ports than measured by the in-stream analysis. These findings indicate that while the flux of water through the main channel at any given time is much higher than the one through the hyporheic zone, a shallow benthic layer with enhanced turnover controls most of the biochemical processing observed at the reach-scale.

From the three MINIPOINT profiles (A, C and D), we determined the extent of the hyporheic zone $\tilde{d}_{hz}$ according to equation (17) and found depths of 9.1, 4.3, and 5.1 cm, respectively (see Table 3). From the reach-scale modeling results, the hyporheic zone was estimated to be on average 8.8 cm deep. Due to the assumptions of the transient storage model, the extent of the reactive storage zone $\tilde{d}_{raz}$ is identical to the total storage zone size if estimated from in-stream results, because the model conceptualizes one single, fully mixed storage zone. However, the subsurface analysis clearly showed that the concentration of resazurin decreased much faster with depth than that of bromide, and the calculated extent of the reactive zone was only about one third of the total depth (approximately 2 cm, see Table 3). This is in agreement with the idea of a highly reactive benthic biolayer close to the streambed, where the majority of compound transformations take place. In our case, this benthic biolayer therefore extended to approximately 2 cm below the streambed, but the actual extent was location-dependent. This also explains why the apparent water ages of resazurin $\tilde{\tau}_{reac}$ are much smaller than those of the conservative tracer $\tilde{\tau}_{hz}$ (Table 3).

Conceptual differences between the two models can also explain why the values obtained for water ages differ greatly (see Table 3). While the in-stream model provides information on the hyporheic travel time distribution (i.e., the age of the water returning to the stream), the subsurface approach determines the hyporheic residence time distribution (i.e., the age of the water at a specific observation point within the hyporheic zone). The obtained quantities of the water ages therefore provide information on how long solute particles have stayed in the hyporheic zone when they return to the stream, or how long a solute particle has stayed in the hyporheic zone while it is still therein, but never both. Because most of the old solute particles found at the deepest ports of the MINIPOINT samplers probably never made it back to the stream (at least not within the timeframe of our experiment), the water age from the in-stream results was much lower than the ages obtained from the subsurface approach. Thus, the majority of the hyporheic exchange

Table 3. Calculated Mean Water Age in the Hyporheic Zone of the Conservative and Reactive Tracer, $\tilde{\tau}_{hz}$ and $\tilde{\tau}_{reac}$, Mean Hyporheic Zone Depths, $\tilde{d}_{hz}$ and $\tilde{d}_{raz}$, Fractions of Tracer loss, f^{tot}_{reac}, Highest Decay Coefficients of Resazurin Obtained for the Given Sampler, $\lambda_{1,max}$, and Hyporheic Exchange Rates at the Stream-Bed Interface, q_{he}[a]

	In-Stream	A	C	D
$\tilde{\tau}_{hz}$ (min)	21.9 ± 2.2	246.8 ± 15.7	51.8 ± 15.1	45.8 ± 2.6
$\tilde{\tau}_{reac}$ (min)	(21.9 ± 2.2)[a]	4.9 ± 7.1	21.2 ± 4.3	3.4 ± 4.4
$\tilde{d}_{hz}$ (cm)	8.8 ± 0.2	9.1 ±0.2	4.3 ± 0.01	5.1 ± 0.03
$\tilde{d}_{raz}$ (cm)	(8.8 ± 0.2)[a]	1.7 ± 0.1	2.2 ± 0.1	1.5 ± 0.2
f^{tot}_{reac}	0.52 ± 2.9e-2	0.81 ± 1.3e-2	0.47 ± 2.1e-2	0.71 ± 2.9e-2
$\lambda_{1,max}$ (1/s)	4.0e-4 ± 3.5e-5	2.9e-3 ± 1.7e-4	2.4e-3 ± 1.7e-4	5.9e-3 ± 3.5e-4
q_{he} (1/s)	1.1e-4 ± 8.9e-6	7.6e-7 ± 1.2e-6	2.5e-6± 4.0e-8	6.0e-6 ± 2.3e-6

[a]The in-stream model does not differentiate between total and reactive depth, but rather assumes a perfectly mixed hyporheic storage zone, for which reason a reactive depth cannot be calculated from this model.

likely happened across the top few centimeters of the streambed, which is also the biolayer portion of the hyporheic zone.

Contributions of the longer flow paths in the subsurface, on the other hand, were of small significance to the reach-scale mass balance. Even though the hyporheic zone is in reality made up of layers with water of different ages and concentrations, the theoretical transient storage model samples water from different ages with the same probability. For catchment-scale transport, it has been recognized that the outlet of a system selects water of different ages within the system in a nonuniform manner, explaining differences between residence and travel-time distributions [*Botter et al*., 2011; *Rinaldo et al*., 2015]. It should also be expected that streams select the age distribution of the hyporheic zone in a nonuniform way. However, the conceptual model of the hyporheic zone as a well-mixed reactor does not allow that.

The hyporheic exchange rates q_{he} differed greatly between in-stream and subsurface analysis, and also among the subsurface results (see Table 3). The difference between the in-stream and subsurface rates was mainly due to a conceptual difference of how hyporheic exchange is quantified. For the subsurface profiles, this exchange rate is related to the advective velocity only, whereas the in-stream approach implicitly lumps advective, dispersive effects, and effect of pressure gradients caused by surface water flow patterns.

In summary, neither in-stream nor subsurface analyses can provide a full picture of the relevant processes. Instead, each approach provides a snapshot of two different parts of the system (see also Figures 1b and 1c). The subsurface analysis revealed that biogeochemical reactions were concentrated in shallow biolayers and indicated how reaction rates decreased with depth. This extent of the benthic biolayer, however, could not be identified from the in-stream analysis because it could not separate the reactive part of the hyporheic zone from nonreactive parts. Nonetheless, it was able to identify the part of the hyporheic reactions essential for reach-scale water chemistry, whereas the subsurface analysis could not provide any information about the relevance of the detected processes on in-stream conditions. These findings are in agreement with a study by *Harvey et al*. [1996] who used a combined surface and subsurface analysis and found that the in-stream tracer was able to characterize the relatively fast exchange between the stream and gravel streambed but failed to account for slower exchange with deeper alluvium. Similarly, *Harvey et al*. [2013], *González-Pinzón et al*. [2015], and *Zarnetske et al*. [2015] concluded that hyporheic zone characteristics cannot be inferred from reach-scale tracer tests alone.

Therefore, subsurface and in-stream results inform about two different parts of the system. Depth profiles provide detailed information about in-situ conditions but contain no information about what the river sees. In-stream results, on the other hand, tell us nothing about the specific location of reaction, but provide integrated information about the reaction zones which have the largest impact on downstream water chemistry.

4. Conclusions

This study contrasted reach-scale tracer tests using bromide (conservative) and resazurin (bioreactive) with simultaneous multisite and multidepth subsurface sampling to quantify coupled transport and reaction at the reach and centimeter-scale. The subsurface approach provided a detailed look at the vertical resolution of hyporheic processes, enabling us to identify layers of higher and lower reactivity from the reaction rates of resazurin, which indicates the importance of the benthic biolayer in controlling substrate supply and subsequent microbial metabolism. While our data helped us to localize layers with increased turnover, they did not allow us to quantitatively resolve the relationship between biomass abundance and function, and hydrological substrate supply.

Even though the benthic biolayer was found to be on average 2 cm thick based on the integrative approach of the reaction depth $\tilde{d}_{raz}$ (according to equation (21)), our analysis showed that the regions of highest metabolic activity are not necessarily located at very shallow depths of the subsurface, but may be found slightly beneath the stream bed at some locations. This pattern and its magnitude is highly location-dependent, and further research is needed to determine whether spatial variations are linked to variations in streambed morphology, or rather an effect of depth-dependent biomass and organic carbon content.

Subsurface profiles alone only resolve a part of the flow paths, and therefore provide little information about water returning to the stream. For this reason, they cannot separate subsurface processes relevant

for whole-stream conditions from those without great significance on the reach scale. The reach-scale approach, on the other hand, is often favored for its spatial integration as it determines an effective reaction rate for the stream reach, but it cannot resolve the importance of specific subsurface processes such as biolayer dynamics that may be relevant for evaluating restoration projects. This outcome agrees with the conclusions of *Harvey et al*. [2013] that reach-scale tracer tests alone are not a suitable tool to quantify the depth of the reaction and the reaction rate in the subsurface, and is also in agreement with studies by *Lemke et al*. [2013a], *González-Pinzón et al*. [2015], and others who showed that in-stream tracer tests are very effective for the determination of bulk reaction rates.

Thus, the subsurface data detects profiles of reactivity within the hyporheic zone, while the reach-scale data reliably estimates whole-stream effects. Conversely, the reach-scale approach cannot constrain the distribution of reactivity in the subsurface when used alone, while depth profiles tell us nothing about water returning from the subsurface to the stream and have therefore little relevance for reach-scale chemistry. Combining approaches adds information about hydrologic and chemical process variability on the different scales, thus illustrating the fundamental discrepancies of the two approaches, owing to the complementary information about hyporheic transport gained by combining the two different types of observation. Combining both types of information with process models of river and hyporheic flow has the potential to vastly improve understanding about the controlling processes and cumulative effects of hyporheic-zone reactions in large drainage basins [*Gomez-Velez et al*., 2015], which will be needed to forecast how changing land use will affect river water quality and to prioritize effective management [*Hester and Gooseff*, 2010; *Mortensen et al*., 2016].

Acknowledgments

J.L.A.K. was supported as a visiting scientist at the U.S. Geological Survey in Reston, VA, USA by the German Academic Exchange Service (DAAD) through a DAAD Doctoral Scholarship and by a Carl Zeiss Stiftung scholarship for Ph.D. research. Further support came from NSF grants EAR 08-38338 and HRD-1345169 (R.G.P.), NSF grant EAR 08-10140 (J.D.D.), and NSF grant EAR 08-14990, and the USGS National Water Quality and Water Availability and Use Programs (J.W.H. and L.G.L.). We thank Roy Haggerty for his collaboration with logistics and early discussions regarding this work and Alexandra Gessner for many helpful comments on this manuscript and we are grateful to Fulvio Boano and three anonymous reviewers for their helpful comments and constructive suggestions. The authors also wish to thank the following people for help with field and laboratory work: Jay Choi, Morgan Maglio, Trevor Langston, Craig Snyder, and Melissa Reardon. The data used are available upon request from the first or last author. Any use of trade, firm, or product names is for descriptive purposes only and does not imply endorsement by the U.S. Government.

References

Argerich, A., R. Haggerty, E. Marti, F. Sabater, and J. Zarnetske (2011), Quantification of metabolically active transient storage (MATS) in two reaches with contrasting transient storage and ecosystem respiration, *J. Geophys. Res.*, *116*, G03034, doi:10.1029/2010JG001379.

Arnon, S., K. Yanuka, and A. Nejidat (2013), Impact of overlying water velocity on ammonium uptake by benthic biofilms, *Hydrol. Processes*, *27*(4), 570–578.

Bardini, L., F. Boano, M. B. Cardenas, R. Revelli, and L. Ridolfi (2012), Nutrient cycling in bedform induced hyporheic zones, *Geochim. Cosmochim. Acta*, *84*, 47–61.

Battin, T. J., L. A. Kaplan, J. D. Newbold, and C. M. Hansen (2003), Contributions of microbial biofilms to ecosystem processes in stream mesocosms, *Nature*, *426*(6965), 439–442.

Battin, T. J., K. Besemer, M. M. Bengtsson, A. M. Romani, and A. I. Packmann (2016), The ecology and biogeochemistry of stream biofilms, *Nat. Rev. Microbiol.*, *14*(4), 251–263.

Bencala, K. E., and R. A. Walters (1983), Simulation of solute transport in a mountain pool-and-riffle stream: A transient storage model, *Water Resour. Res.*, *19*(3), 718–724.

Bhaskar, A. S., J. W. Harvey, and E. J. Henry (2012), Resolving hyporheic and groundwater components of streambed water flux using heat as a tracer, *Water Resour. Res.*, *48*, W08524, doi:10.1029/2011WR011784.

Boano, F., J. W. Harvey, A. Marion, A. I. Packman, R. Revelli, L. Ridolfi, and A. Wörman (2014), Hyporheic flow and transport processes: Mechanisms, models, and biogeochemical implications, *Rev. Geophys.*, *52*, 603–679, doi:10.1002/2012RG000417.

Böhlke, J. K., R. C. Antweiler, J. W. Harvey, A. E. Laursen, L. K. Smith, R. L. Smith, and M. A. Voytek (2009), Multi-scale measurements and modeling of denitrification in streams with varying flow and nitrate concentration in the upper Mississippi River basin, USA, *Biogeochemistry*, *93*(1-2), 117–141.

Botter, G., E. Bertuzzo, and A. Rinaldo (2011), Catchment residence and travel time distributions: The master equation, *Geophys. Res. Lett.*, *38*, L11403, doi:10.1029/2011GL047666.

Boulton, A. J., S. Findlay, P. Marmonier, E. H. Stanley, and H. M. Valett (1998), The functional significance of the hyporheic zone in streams and rivers, *Annu. Rev. Ecol. Syst.*, *29*, 59–81.

Briggs, M. A., L. K. Lautz, D. K. Hare, and R. González-Pinzón (2013), Relating hyporheic fluxes, residence times, and redox-sensitive biogeochemical processes upstream of beaver dams, *Freshwater Sci.*, *32*(2), 622–641.

Briggs, M. A., F. D. Day-Lewis, J. P. Zarnetske, and J. W. Harvey (2015), A physical explanation for the development of redox microzones in hyporheic flow, *Geophys. Res. Lett.*, *42*, 4402–4410, doi:10.1002/2015GL064200.

Brunke, M., and T. Gonser (1997), The ecological significance of exchange processes between rivers and groundwater, *Freshwater Biol.*, *37*(1), 1–33.

Conant, B., J. A. Cherry, and R. W. Gillham (2004), A PCE groundwater plume discharging to a river: Influence of the streambed and near-river zone on contaminant distributions, *J. Contamin. Hydrol.*, *73*(1), 249–279.

Fischer, H., M. Pusch, and J. Schwoerbel (1996), Spatial distribution and respiration of bacteria in stream-bed sediments, *Arch. Hydrobiol.*, *137*(3), 281–300.

Fuller, C. C., and J. W. Harvey (2000), Reactive uptake of trace metals in the hyporheic zone of a mining-contaminated stream, Pinal Creek, Arizona, *Environ. Sci. Technol.*, *34*(7), 1150–1155.

Gomez-Velez, J. D., J. W. Harvey, M. B. Cardenas, and B. Kiel (2015), Denitrification in the Mississippi River network controlled by flow through river bedforms, *Nat. Geosci.*, *8*, 941–945.

González-Pinzón, R., and R. Haggerty (2013), An efficient method to estimate processing rates in streams, *Water Resour. Res.*, *49*, 6096–6099, doi:10.1002/wrcr.20446.

González-Pinzón, R., R. Haggerty, and D. D. Myrold (2012), Measuring aerobic respiration in stream ecosystems using the resazurin-resorufin system, *J. Geophys. Res.*, *117*, G00N06, doi:10.1029/2012JG001965.

Gonzalez-Pinzon, R., R. Haggerty, and A. Argerich (2014), Quantifying spatial differences in metabolism in headwater streams, *Freshwater Sci.*, *33*(3), 798–811.
González-Pinzón, R., A. S. Ward, C. E. Hatch, A. N. Wlostowski, K. Singha, M. N. Gooseff, R. Haggerty, J. W. Harvey, O. A. Cirpka, and J. T. Brock (2015), A field comparison of multiple techniques to quantify groundwater–surface-water interactions, *Freshwater Sci.*, *34*(1), 139–160.
Gooseff, M. N., S. M. Wondzell, R. Haggerty, and J. Anderson (2003), Comparing transient storage modeling and residence time distribution (RTD) analysis in geomorphically varied reaches in the Lookout Creek basin, Oregon, USA, *Adv. Water Resour.*, *26*(9), 925–937.
Grimm, N. B., and S. G. Fisher (1984), Exchange between interstitial and surface water: Implications for stream metabolism and nutrient cycling, *Hydrobiologia*, *111*(3), 219–228.
Haggerty, R., A. Argerich, and E. Marti (2008), Development of a "smart" tracer for the assessment of microbiological activity and sediment-water interaction in natural waters: The resazurin-resorufin system, *Water Resour. Res.*, *44*, W00D01, doi:10.1029/2007WR006670.
Haggerty, R., E. Marti, A. Argerich, D. von Schiller, and N. B. Grimm (2009), Resazurin as a "smart" tracer for quantifying metabolically active transient storage in stream ecosystems, *J. Geophys. Res.*, *114*, G03014, doi:10.1029/2008JG000942.
Harvey, C. F., and S. M. Gorelick (1995), Temporal moment-generating equations: Modeling transport and mass-transfer in heterogeneous aquifers, *Water Resour. Res.*, *31*(8), 1895–1911.
Harvey, J. W., and C. C. Fuller (1998), Effect of enhanced manganese oxidation in the hyporheic zone on basin-scale geochemical mass balance, *Water Resour. Res.*, *34*(4), 623–636.
Harvey, J. W., and M. Gooseff (2015), River corridor science: Hydrologic exchange and ecological consequences from bedforms to basins, *Water Resour. Res.*, *51*, 6893–6922, doi:10.1002/2015WR017617.
Harvey, J. W., B. J. Wagner, and K. E. Bencala (1996), Evaluating the reliability of the stream tracer approach to characterize stream-subsurface water exchange, *Water Resour. Res.*, *32*(8), 2441–2451.
Harvey, J. W., et al. (2012), Hydrogeomorphology of the hyporheic zone: Stream solute and fine particle interactions with a dynamic streambed, *J. Geophys. Res.*, *117*, G00N11, doi:10.1029/2012JG002043.
Harvey, J. W., J. K. Bohlke, M. A. Voytek, D. Scott, and C. R. Tobias (2013), Hyporheic zone denitrification: Controls on effective reaction depth and contribution to whole-stream mass balance, *Water Resour. Res.*, *49*, 6298–6316, doi:10.1002/wrcr.20492.
Hendricks, S. P. (1993), Microbial ecology of the hyporheic zone: A perspective integrating hydrology and biology, *J. N. Am. Benthol. Soc.*, *12*(1), 70–78.
Hester, E. T., and M. N. Gooseff (2010), Moving beyond the banks: Hyporheic restoration is fundamental to restoring ecological services and functions of streams, *Environ. Sci. Technol.*, *44*(5), 1521–1525.
Hollenbeck, K. (1998), *INVLAP. M: A Matlab Function for Numerical Inversion of Laplace Transforms by the de Hoog Algorithm*. [Available at https://www.mathworks.com/matlabcentral/answers/uploaded_files/1034/invlap.m.]
Kerr, P. C., M. N. Gooseff, and D. Bolster (2013), The significance of model structure in one-dimensional stream solute transport models with multiple transient storage zones: Competing vs. nested arrangements, *J. Hydrol.*, *497*, 133–144.
Krause, S., D. Hannah, J. Fleckenstein, C. Heppell, D. Kaeser, R. Pickup, G. Pinay, A. Robertson, and P. Wood (2011), Inter-disciplinary perspectives on processes in the hyporheic zone, *Ecohydrology*, *4*(4), 481–499.
Kucera, E. (1965), Contribution to theory of chromatography linear non-equilibrium elution chromatography, *J. Chromatogr.*, *19*(2), 237–248.
Laloy, E., and J. A. Vrugt (2012), High-dimensional posterior exploration of hydrologic models using multiple-try DREAM (ZS) and high-performance computing, *Water Resour. Res.*, *48*, W01526, doi:10.1029/2011WR010608.
Lemke, D., Z. J. Liao, T. Wohling, K. Osenbruck, and O. A. Cirpka (2013a), Concurrent conservative and reactive tracer tests in a stream undergoing hyporheic exchange, *Water Resour. Res.*, *49*, 3024–3037, doi:10.1002/wrcr.20277.
Lemke, D., P. A. Schnegg, M. Schwientek, K. Osenbruck, and O. A. Cirpka (2013b), On-line fluorometry of multiple reactive and conservative tracers in streams, *Environ. Earth Sci.*, *69*(2), 349–358.
Liao, Z. J., and O. A. Cirpka (2011), Shape-free inference of hyporheic travel time distributions from synthetic conservative and "smart" tracer tests in streams, *Water Resour. Res.*, *47*, W07510, doi:10.1029/2010WR009927.
Liao, Z. J., D. Lemke, K. Osenbruck, and O. A. Cirpka (2013), Modeling and inverting reactive stream tracers undergoing two-site sorption and decay in the hyporheic zone, *Water Resour. Res.*, *49*, 3406–3422, doi:10.1002/wrcr.20276.
Marion, A., M. Zaramella, and A. Bottacin-Busolin (2008), Solute transport in rivers with multiple storage zones: The STIR model, *Water Resour. Res.*, *44*, W10406, doi:10.1029/2008WR007037.
Mortensen, J. G., R. Gonzalez-Pinzoń, C. N. Dahm, J. Wang, L. H. Zeglin, and D. J. Van Horn (2016), Advancing the Food-Energy–Water Nexus: Closing Nutrient Loops in Arid River Corridors, *Environ. Sci. Technol.*, *50*(16), 8485–8496.
Navel, S., F. Mermillod-Blondin, B. Montuelle, E. Chauvet, L. Simon, and P. Marmonier (2011), Water–sediment exchanges control microbial processes associated with leaf litter degradation in the hyporheic zone: A microcosm study, *Microb. Ecol.*, *61*(4), 968–979.
O'Brien, J., I. Wilson, T. Orton, and F. Pognan (2000), Investigation of the Alamar Blue (resazurin) fluorescent dye for the assessment of mammalian cell cytotoxicity, *Eur. J. Biochem.*, *267*(17), 5421–5426.
O'Connor, B. L., and J. W. Harvey (2008), Scaling hyporheic exchange and its influence on biogeochemical reactions in aquatic ecosystems, *Water Resour. Res.*, *44*, W12423, doi:10.1029/2008WR007160.
O'Connor, B. L., and M. Hondzo (2008), Dissolved oxygen transfer to sediments by sweep and eject motions in aquatic environments, *Limnol. Oceanogr.*, *53*(2), 566–578.
O'Connor, B. L., J. W. Harvey, and L. E. McPhillips (2012), Thresholds of flow-induced bed disturbances and their effects on stream metabolism in an agricultural river, *Water Resour. Res.*, *48*, W08504, doi:10.1029/2011WR011488.
Rinaldo, A., P. Benettin, C. J. Harman, M. Hrachowitz, K. J. McGuire, Y. van der Velde, E. Bertuzzo, and G. Botter (2015), Storage selection functions: A coherent framework for quantifying how catchments store and release water and solutes, *Water Resour. Res.*, *51*, 4840–4847, doi:10.1002/2015WR017273.
Rodriguez-Freire, L., S. M. Avasarala, A.-M. S. Ali, D. Agnew, J. H. Hoover, K. Artyushkova, D. E. Latta, E. J. Peterson, J. Lewis, and L. J. Crossey (2016), Post Gold King Mine spill investigation of metal stability in water and sediments of the Animas River watershed, *Environ. Sci. Technol.*, *50*(21), 11539–11548.
Runkel, R. L. (1998), One-dimensional transport with inflow and storage (OTIS): A solute transport model for streams and rivers, *U.S. Geol. Sur. Water Resour. Invest. Rep.*, 98-4018, 73 pp.
Runkel, R. L. (2007), Toward a transport-based analysis of nutrient spiraling and uptake in streams, *Limnol. Oceanogr. Methods*, *5*(1), 50–62.
Sardin, M., D. Schweich, F. J. Leij, and M. T. Vangenuchten (1991), Modeling the nonequilibrium transport of linearly interacting solutes in porous-media: A review, *Water Resour. Res.*, *27*(9), 2287–2307.
Stanford, J., and J. Ward (1988), The hyporheic habitat of river ecosystems, *Nature*, *335*, 64–66.

Triska, F. J., V. C. Kennedy, R. J. Avanzino, G. W. Zellweger, and K. E. Bencala (1989), Retention and transport of nutrients in a third-order stream in northwestern California: Hyporheic processes, *Ecology*, *70*, 1893–1905.

Vrugt, J. A., C. Ter Braak, C. Diks, B. A. Robinson, J. M. Hyman, and D. Higdon (2009), Accelerating Markov chain Monte Carlo simulation by differential evolution with self-adaptive randomized subspace sampling, *Int. J. Nonlinear Sci. Numer. Simul.*, *10*(3), 273–290.

Wörman, A. (1998), Analytical solution and timescale for transport of reacting solutes in rivers and streams, *Water Resour. Res.*, *34*(10), 2703–2716.

Wörman, A., A. I. Packman, H. Johansson, and K. Jonsson (2002), Effect of flow-induced exchange in hyporheic zones on longitudinal transport of solutes in streams and rivers, *Water Resour. Res.*, *38*(1), 1001, doi:10.1029/2001WR000769.

Zaramella, M., A. I. Packman, and A. Marion (2003), Application of the transient storage model to analyze advective hyporheic exchange with deep and shallow sediment beds, *Water Resour. Res.*, *39*(7), 1198, doi:10.1029/2002WR001344.

Zarnetske, J. P., R. Haggerty, and S. M. Wondzell (2015), Coupling multiscale observations to evaluate hyporheic nitrate removal at the reach scale, *Freshwater Sci.*, *34*(1), 172–186.